Published in IET Electrical Systems in Transportation
Received on 7th April 2011
Revised on 11th November 2011
doi: 10.1049/iet-est.2011.0021

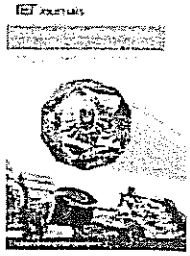

ISSN 2042-9738

Self-regulating particle swarm optimised controller for (photovoltaic–fuel cell) battery charging of hybrid electric vehicles

A.A.A. Elgammal A.M. Sharaf

Centre for Energy Studies, University of Trinidad and Tobago, Pt. Lisas Campus, Esperanza Road, Brechin Castle, Trinidad and Tobago
E-mail: adel.elgammal@utt.edu.tt; adel.sharaf@utt.edu.tt

Abstract: This study presents the use of hybrid photovoltaic–fuel cell (PV–FC) renewable energy scheme for vehicle-to-grid (V2G) battery-charging stations. The hybrid PV–FC DC interface scheme is dynamically controlled using a self-regulating tri-loop controller based on multi-objective particle swarm optimisation. The proposed utilisation scheme ensures efficient DC source energy utilisation from the hybrid PV–FC DC with minimal DC current inrush conditions and a fully stabilised DC bus voltage. The multi-loop battery-charging regulator allows for hybrid (voltage, current and power) charging modes for efficient, fast charging and DC energy efficient utilisation. The proposed hybrid renewable green energy PV–FC battery-charging scheme is fully validated by simulation and laboratory prototype testing.

Nomenclature

PSO	particle swarm optimisation
SOPSO	single-objective particle swarm optimisation
MOPSO	multi-objective particle swarm optimisation
FC	fuel cell
PV	photo voltaic
HEV	hybrid electric vehicle
GPFC	green plug filter compensator
V_{id}	velocity of the ith particle with d dimensions
X_{id}	position of the ith particle with d dimensions
rand_1, rand_2	two uniform random functions on the range [0.1]
ω	inertia weight that is chosen beforehand
C_1	cognitive learning rate
C_2	social learning rate
P_{id}	location along dimension d at which the particle previously had the best-fitness measure
P_{gd}	current location along dimension d of the neighbourhood particle with the best fitness
V_d	instantaneous DC bus voltage
$V_{d\ \text{base}}$	base value of the DC bus voltage
I_d	instantaneous DC bus current
$I_{d\ \text{base}}$	base value of the DC bus current
T_{12}, T_{13}, T_{14}	time delays for the green plug filter compensator scheme regulator (B)
V_B	instantaneous battery voltage
$V_{B\ \text{base}}$	base value of the battery voltage
I_B	instantaneous battery current
$I_{B\ \text{base}}$	base value of the battery current
T_1–T_9	time delays for the DC boost chopper regulator (A) scheme
T_{10},T_{11}	time delays for the energy management regulator (C) scheme
D	time-delay loop
K_P, K_I, K_D γ_1, γ_2	self-tuned weighted modified proportional-integral-derivative (PID) controller gains

1 Introduction

As the public concerns about the pollutions and global warming produced by fossil fuel engines increases and the demand for renewable and green energy increases, alternative and sustainable transportation methods become more attractive in comparison to conventional fossil-fuel-based transportation [1, 2]. However, renewable green energy sources such as wind turbine generators and photovoltaic are intermittent in nature, and produce fluctuating active power. Interconnecting these intermittent sources to the utility grid at a large scale may affect the voltage/frequency control of the grid, and may lead to severe power quality issues [3]. Different electric vehicles (EV), plug-in hybrid electric vehicles (PHEV) and hybrid EVs are considered as viable alternatives to reduce the current fleet of fossil-fuel-driven vehicles and reduce the air pollution in densely populated metropolitan areas [4, 5]. The PHEV is a

hybrid vehicle with a storage system that can be recharged by connecting the vehicle plug to an external electric power source [6]. The increasing use of EVs will inevitably prompt the use of a large number of battery chargers to supply the dc voltage required to charge battery packs [7]. Because of their limited energy capacity, EV batteries need frequent recharge, and it is usually desirable to do this as rapidly as possible [8, 9]. The ability to reduce the charging time depends on delivering as much current as possible during the charging period. The parameters that ultimately limit the charging current are (i) the current capacity of the ac source, (ii) the thermal limitations of the charger and (iii) the thermal and chemical limitations of the battery [10, 11]. Different battery types, charging schemes and classes were proposed [12–20]. A new battery-charging scheme and control strategy using photo voltaic (PV) systems is based on a dynamic EMS-energy management algorithm to directly connect or disconnect the solar array modules to the battery bank [13–15]. Consequently, the battery full capacity is not reached. In order to achieve the full capacity without causing overheating or overcharge, an alternative charging method based on on/off control is proposed in [16–18]. Consequently, the available maximum renewable energy is not fully utilised and energy utilisation is severely compromised during the off-time, no energy is transferred to the battery. Another method proposed a battery-charging algorithm based on the state of the charge (SOC) using an estimator [19, 20], but accurate estimation of the battery SOC remains very complex and is difficult to be implemented because of battery limited models and parametric uncertainties. The objective of this paper is to design an efficient battery charger controller fed from hybrid FC–PV renewable green energy sources, so that the PV can be used as an additional energy source for hybrid EV using FC. The self-regulating battery charger controller is proposed based on multi-objective particle swarm optimisation (MOPSO) and gain-adjusting search algorithm. The battery charger is controlled by tri-loop error-driven regulators to operate at the unity power factor and with reasonable harmonics, especially no low-order harmonics. The battery charger has efficient charging hybrid characteristics such as constant current and/or constant voltage mode. The goal of the MOPSO regulators is to minimise the charging time, total harmonic distortion (THD), improve utilisation of the hybrid FC–PV renewable energy and maximise the DC power available from the hybrid FC–PV renewable energy sources during the fast-charging period.

2 MOPSO

Particle swarm optimisation (PSO) is an evolutionary soft computational optimisation technique (a search method based on a natural system) developed by Kennedy and Eberhart [21]. The system initially has a population of random selective solutions. Each potential solution is called a particle. Each particle is given a random velocity and is flown through the problem space. The particles have memory and each particle keeps track of its previous best position (called the P_{best}) and its corresponding fitness. There exist a number of P_{best} for the respective particles in the swarm and the particle with greatest fitness is called the global best (G_{best}) of the swarm. The basic concept of the PSO technique lies in accelerating each particle towards its P_{best} and G_{best} locations, with a random weighted acceleration at each time step.

A multi-objective search and optimisation problem are defined as any optimisation problem that have more than

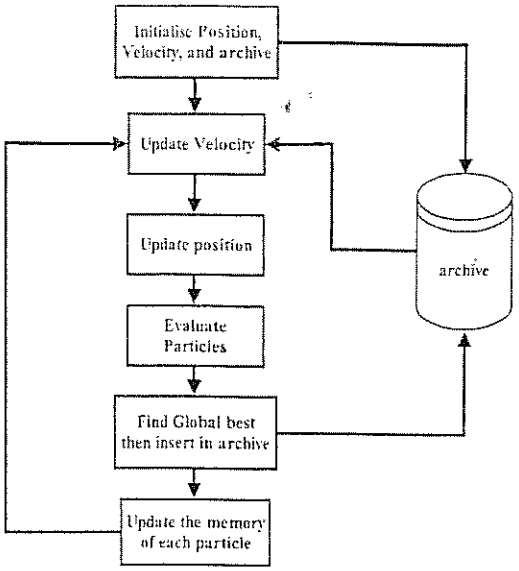

Fig. 1 *Flow chart of the MOPSO optimisation search algorithm*

one desired solution or final objective and all objectives are normally in conflict with respect to each other, which means that there is no one optimal solution [22]. Instead, there are sets of compromises or 'trade-off' near-optimal solutions that can be utilised based on desired features or accepted compromises among the objectives [22].

In MOPSO [22–24], a set of particles are initialised in the decision space at random. For each particle i, a position x_i in the decision space and a velocity v_i are assigned. The particles change their positions and move towards the so far best-found solutions. The non-dominated solutions from the last generations are kept in the archive. The archive is an external population, in which the so far found non-dominated solutions are kept. Moving towards the optima is done in the calculations of the velocities as follows

$$V_{id} = \omega \times V_{id} + C_1 \times \text{rand}_1 \times (P_{pd} - X_{id}) + C_2 \times \text{rand}_2 \times (P_{rd} - X_{id}) \quad (1)$$

$$X_{id} = X_{id} + V_{id} \quad (2)$$

where P_{rd}, P_{pd} are randomly chosen from a single global Pareto archive, ω is the inertia factor influencing the local and global abilities of the algorithm, $V_{i,d}$ is the velocity of the particle i in the dth dimension, c_1 and c_2 are weights affecting the cognitive and social factors, respectively. r_1 and r_2 are two uniform random functions in the range [0, 1]. According to (6), each particle has to change its position X_{id} towards the position of the two guides P_{rd}, P_{pd}, which must be selected from the updated set of non-dominated solutions stored in the archive. The particles change their positions during generations until a termination criterion is met. Fig. 1 shows the flow chart of the MOPSO.

3 System description

The PV–FC sample study scheme shown in Fig. 2 comprises a hybrid PV–FC utilisation scheme with a common DC interface bus feeding a buck-boost DC–DC converter for battery-charging station. Auxiliary loads (heating, lighting, DC motor for ventilation and air conditioning) are located at the common DC Bus (V_d), which is further stabilised by

doi: 10.1049/iet-est.2011.0021

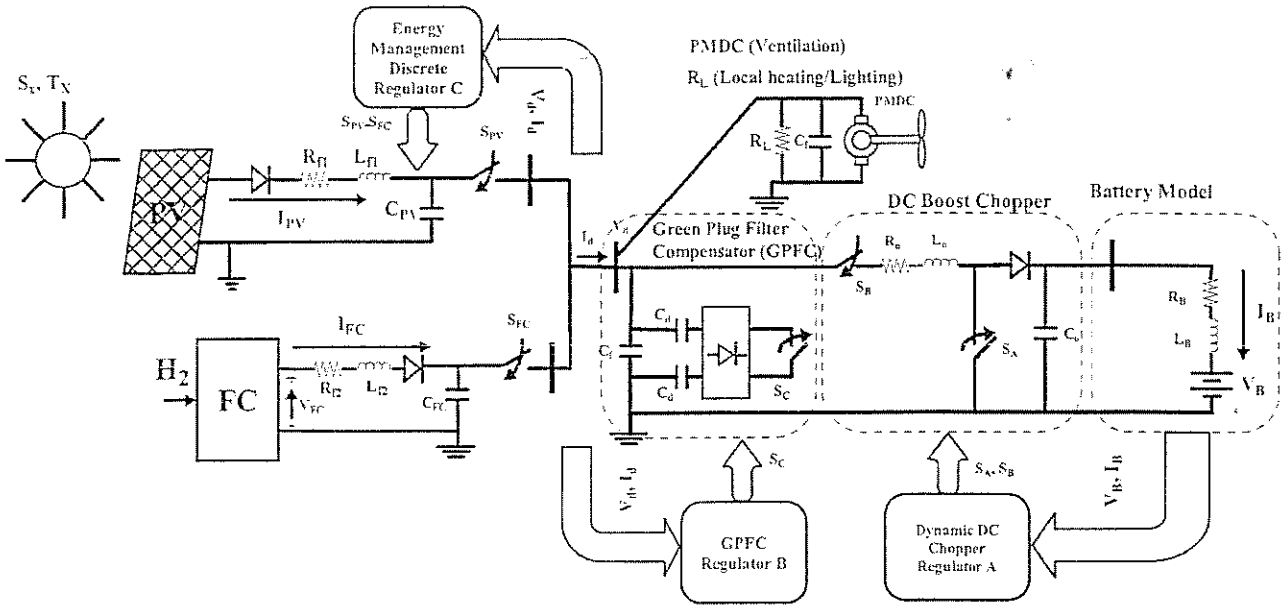

Fig. 2 *Schematic diagram of the hybrid renewable green energy PV–FC battery-charging station with tri-regulator coordinated controller*

a novel green plug filter compensator (GPFC). The DC renewable energy utilisation scheme is regulated by multi-loop regulation (A, B and C) schemes, as shown in Figs. 3–5, for energy management of PV and FC DC energy sources, common DC bus voltage stabilisation and efficient flexible mode battery charging. The proposed dynamic tri-loop error-driven controller is an advanced regulation concept that operates as an adaptive dynamic type multi-purpose controller capable of handling sudden parametric changes, load and/or DC source excursions. The common concerns of power quality issues include duration voltage variations (overvoltage, under-voltage and sustained interruptions), short-duration voltage variations (interruption, sags and swells), voltage imbalance (voltage unbalance), waveform distortion (DC offset, harmonics, inter-harmonics, notching and noise), voltage fluctuation (voltage flicker) and power frequency variations. To prevent any undesirable transients and inrush current, a GPFC scheme is used to ensure stable, efficient, minimal inrush operation of the hybrid renewable energy scheme.

The global error is the summation of the three-loop individual errors including voltage stability, current limiting and synthesise dynamic power loops. Each multi-loop dynamic control scheme is used to reduce a global error based on a tri-loop dynamic error summation signal and to mainly track a given voltage reference. The DC buck-boost chopper regulates the battery-charging voltage or current according to the selected charging mode. In the current regulation loop, the weighted modified PID controller is used to regulate the charging current and its output, so that the charging current ripple is reduced.

A number of conflicting objective functions are selected to optimise and select best controller gains using the PSO algorithm. These functions are defined by the following

$$J1 = \text{minimise the charging time} \tag{3}$$

The objective is to ensure fast charging time of the battery without overheating. The battery charger controller continually monitors battery voltage. When battery voltage,

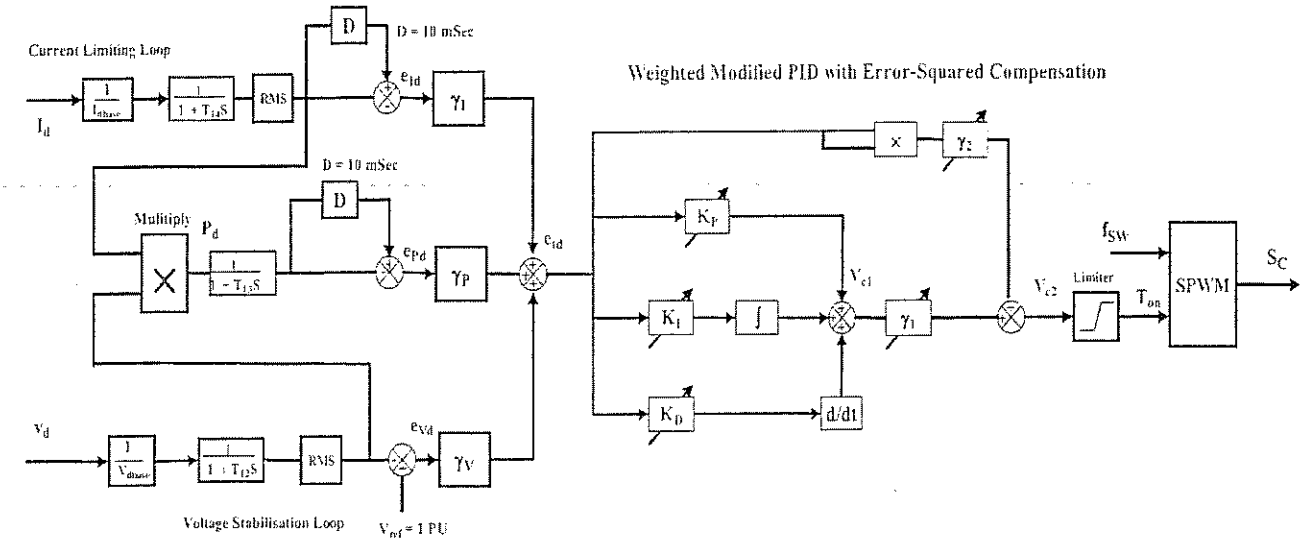

Fig. 3 *Tri-loop error-driven self-regulating weighted modified PID regulator (B) for the DC-bus GPFC filter compensator scheme*

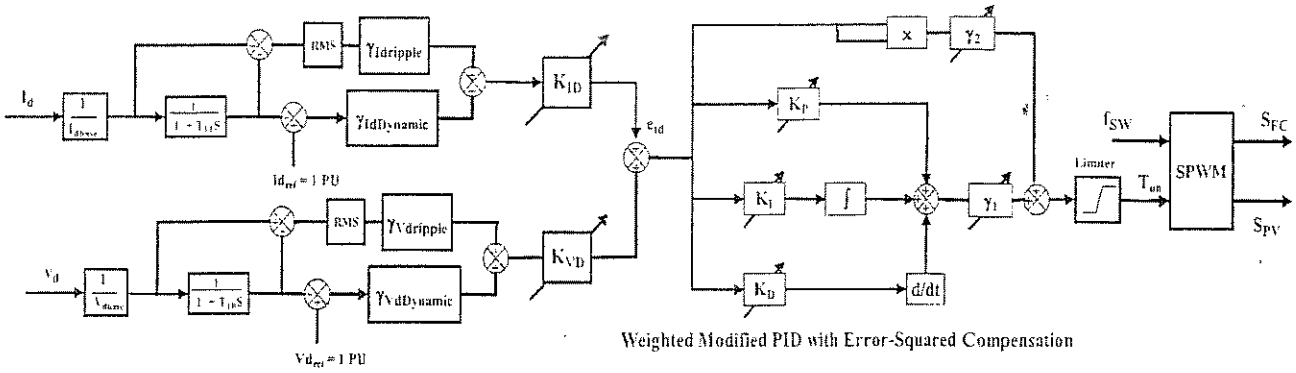

Fig. 4 *Tri-loop error-driven self-regulating weighted modified PID regulator (C) for the renewable energy management scheme*

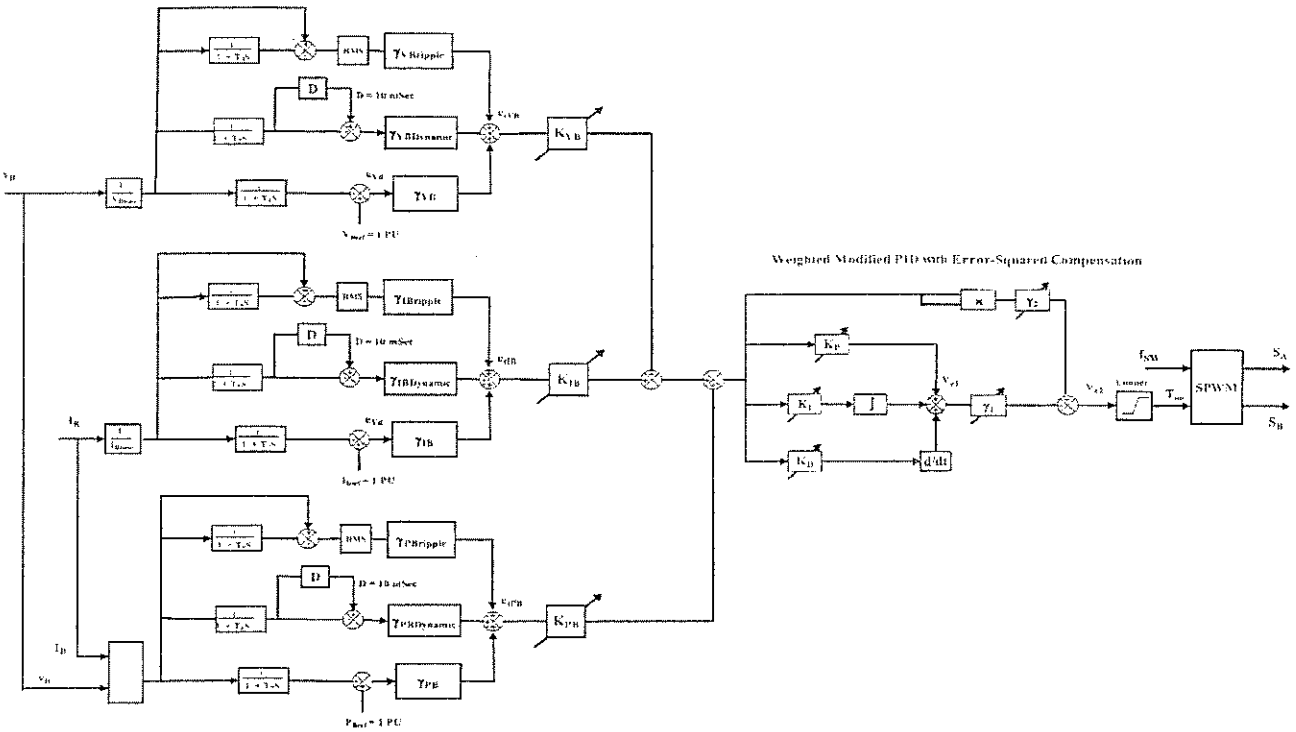

Fig. 5 *Tri-loop error-driven self-regulating modified PID regulator (A) for hybrid multi-mode battery-charging chopper*

reaches a peak and subsequent decrease, charge is terminated. This typically occurs at 85–95% of full battery charge

$$J2 = \text{minimise the THD} \tag{4}$$

The objective is to reduce the THD and fluctuations/variations in the common DC collection system by limiting DC bus V_d transients and ripple content. The THD of a waveform is calculated by taking the square root of the addition of the squares of the harmonic currents, and dividing them by the fundamental component. As a formula

$$\text{THD}_{V_d} = \frac{\sqrt{\sum_{n=2}^{\infty} V_{dn}^2}}{V_{d1}} \tag{5}$$

where THD_{Vd} is the THD of the DC bus voltage and V_{d1}, V_{d2}, V_{d3}, V_{d4}, V_{d5} ... are the DC bus voltages at their respective harmonics.

$$\text{THD}_{I_d} = \frac{\sqrt{\sum_{n=2}^{\infty} I_{dn}^2}}{I_{d1}} \tag{6}$$

where THD_{Id} is the THD of the DC bus current and I_{d1}, I_{d2}, I_{d3}, I_{d4}, I_{d5}, ... are the DC bus currents at their respective harmonics.

$$J3 = \text{maximise the battery charger efficiency} \tag{7}$$

The battery-charging efficiency is improved by reducing system and battery losses and ensuring an effective charging pattern based on the hybrid battery: voltage–current–power reference tracking. The losses are device losses, which are directly proportional to the output current of the charger since the voltage drop across the devices is basically constant during conduction.

doi: 10.1049/iet-est.2011.0021

To calculate the charging efficiency, we have to record the charging and discharging capacity; the charging efficiency is calculated as

$$\eta\% = \frac{\int_{t_{do}}^{t_{df}} i_d(t)\,dt}{\int_{t_{co}}^{t_{cf}} i_c(t)\,dt} \tag{8}$$

where $i_c(t)$ is the charging current and $i_d(t)$ is the discharging current, t_{co} is the initial charging time, t_{cf} is the final charging time, t_{do} is the initial discharging time and t_{df} is the final discharging time

$$J4 = \text{minimise the global error of all regulators} \tag{9}$$

The dynamic error-driven absolute errors of all control-regulators $\{e_{id1}, e_{id2}, e_{iB}\}$ is minimised dynamically to ensure effective tracking and minimal excursions.

The (per-unit) three-dimensional-error vector (e_{vd1}, e_{Id1}, e_{pd1}) of the GPFC scheme is governed by the following equations

$$e_{vd1}(k) = 1 - \text{RMS}\left(\left(\frac{V_d(k)}{V_{d\,\text{base}}}\right) \times \left(\frac{1}{1+ST_{12}}\right)\right) \tag{10}$$

$$e_{Id1}(k) = \text{RMS}\left(\left(\frac{I_d(k)}{I_{d\,\text{base}}}\right) \times \left(\frac{1}{1+ST_{14}}\right)\right) \times \left(\left(\frac{1}{1+SD}\right) - 1\right) \tag{11}$$

$$e_{Pd1}(k) = \left(\text{RMS}\left(\left(\frac{V_d(k)}{V_{d\,\text{base}}}\right) \times \left(\frac{1}{1+ST_{12}}\right)\right)\right) \times \left(\text{RMS}\left(\left(\frac{I_d(k)}{I_{d\,\text{base}}}\right) \times \left(\frac{1}{1+ST_{14}}\right)\right)\right) \times \left(\frac{1}{1+ST_{13}}\right) \times \left(\left(\frac{1}{1+SD}\right) - 1\right) \tag{12}$$

Moreover, the total or global error e_{id1} (k) for the DC side GPFC scheme at a time instant:

$$e_{id1}(k) = \gamma_{vd} e_{vd1}(k) + \gamma_{id} e_{id1}(k) + \gamma_{pd} e_{pd1}(k) \tag{13}$$

The (per-unit) three-dimensional-error vector (e_{vd2}, e_{Id2}) of the renewable energy management scheme is governed by the following equations

$$e_{vd2}(k) = \gamma_{V\,\text{dynamic}} \times \left(1 - \left(\left(\frac{V_d(k)}{V_{d\,\text{base}}}\right) \times \left(\frac{1}{1+ST_{10}}\right)\right)\right) + \gamma_{Vd\,\text{ripple}} \times \text{RMS}\left(\frac{V_d(k)}{V_{d\,\text{base}}}\right) - \left(\left(\frac{V_d(k)}{V_{d\,\text{base}}}\right) \times \left(\frac{1}{1+ST_{10}}\right)\right) \tag{14}$$

$$e_{Id2}(k) = \gamma_{I\,\text{dynamic}} \times \left(1 - \left(\left(\frac{I_d(k)}{I_{d\,\text{base}}}\right) \times \left(\frac{1}{1+ST_{11}}\right)\right)\right) + \gamma_{Id\,\text{ripple}} \times \text{RMS}\left(\frac{I_d(k)}{I_{d\,\text{base}}}\right) - \left(\left(\frac{I_d(k)}{I_{d\,\text{base}}}\right) \times \left(\frac{1}{1+ST_{11}}\right)\right) \tag{15}$$

Moreover, the total or global error e_{id2} (k) for the renewable energy management scheme at a time instant

$$e_{id2}(k) = K_{vd} e_{vd2}(k) + K_{id} e_{id2}(k) \tag{16}$$

The (per-unit) three-dimensional-error vector (e_{vB}, e_{IB}, e_{PB}) for hybrid multi-mode battery-charging chopper is governed by the following equations

$$e_{vB}(k) = \gamma_{V\,\text{B dynamic}} \times \left(\left(\left(\frac{V_B(k)}{V_{B\,\text{base}}}\right) \times \left(\frac{1}{1+ST_2}\right)\right) \times \left(\left(\frac{1}{1+SD}\right) - 1\right)\right) + \gamma_{V\,\text{B}d\,\text{ripple}} \times \text{RMS}\left(\frac{V_B(k)}{V_{B\,\text{base}}}\right) - \left(\left(\frac{V_B(k)}{V_{B\,\text{base}}}\right) \times \left(\frac{1}{1+ST_3}\right)\right) + \gamma_{V\,\text{B}}\left(1 - \left(\left(\frac{V_B(k)}{V_{B\,\text{base}}}\right) \times \left(\frac{1}{1+ST_1}\right)\right)\right) \tag{17}$$

$$e_{IB}(k) = \gamma_{I\,\text{B dynamic}} \times \left(\left(\left(\frac{I_B(k)}{I_{B\,\text{base}}}\right) \times \left(\frac{1}{1+ST_5}\right)\right) \times \left(\left(\frac{1}{1+SD}\right) - 1\right)\right) + \gamma_{I\,\text{B}d\,\text{ripple}} \times \text{RMS}\left(\frac{I_B(k)}{I_{B\,\text{base}}}\right) - \left(\left(\frac{I_B(k)}{I_{B\,\text{base}}}\right) \times \left(\frac{1}{1+ST_6}\right)\right) + \gamma_{I\,\text{B}}\left(1 - \left(\left(\frac{I_B(k)}{I_{B\,\text{base}}}\right) \times \left(\frac{1}{1+ST_4}\right)\right)\right) \tag{18}$$

$$e_{PB}(k) = \gamma_{P\,\text{B dynamic}} \times \left(\left(\left(\frac{V_B(k) \times I_B(k)}{V_{\text{Base}} \times I_{B\,\text{base}}}\right) \times \left(\frac{1}{1+ST_8}\right)\right) \times \left(\left(\frac{1}{1+SD}\right) - 1\right)\right) + \gamma_{P\,\text{B}d\,\text{ripple}} \times \text{RMS}\left(\frac{V_B(k) \times I_B(k)}{V_{\text{Base}} \times I_{B\,\text{base}}}\right) - \left(\left(\frac{V_B(k) \times I_B(k)}{V_{\text{Base}} \times I_{B\,\text{base}}}\right) \times \left(\frac{1}{1+ST_9}\right)\right) + \gamma_{P\,\text{B}}\left(1 - \left(\left(\frac{V_B(k) \times I_B(k)}{V_{\text{Base}} \times I_{B\,\text{base}}}\right) \times \left(\frac{1}{1+ST_7}\right)\right)\right) \tag{19}$$

And the total or global error $e_{i\,B}$ (k) for the renewable energy management scheme at a time instant

$$e_{i\,B}(k) = K_{vB} e_{vB}(k) + K_{iB} e_{iB}(k) + K_{PB} e_{PB}(k) \tag{20}$$

$$J_5 = \text{maximise the available DC power from PV} - \text{FC} \tag{21}$$

The total power collected at DC bus V_d is maximised under excursions in PV and FC DC sources because of changes in irradiation, ambient temperature or volt–ampere non-linear characteristics because of sudden excursions.

$$P_d = V_d I_d \tag{22}$$

In general, to solve this complex optimality search problem, there are two possible optimisation techniques based on

particle swarm optimisation (PSO): single aggregate selected objective optimisation and MOPSO. The main procedure of the single aggregate selected objective optimisation is based on selecting a single aggregate objective function with weighted single-objective parameters scaled by a number of weighting factors. The objective function is optimised (either minimised or maximised) using PSO to obtain a single global or near-optimal solution. On the other hand, the main objective of the MOPSO problem is finding the set of acceptable (trade-off) optimal solutions. This set of accepted solutions is called Pareto front. MOPSO hybrid-objective function is a multi stage number of cascaded objective functions that are optimised in succession using the minimal deviation or absolute error criteria. The final near-optimal solution (Pareto-surfaces) represents a near compromise of all objective functions, especially conflicting objective functions. The main advantages of the proposed MOPSO method are: it does not require a priori knowledge of the relative importance of the objective functions, and it provides a set of acceptable trade-off near-optimal solutions. Both PSO and MOPSO searching algorithms are tested, validated and compared.

4 Digital simulation results

The EV battery charger scheme using the PV–FC renewable generation system performance is compared for two cases, with fixed and self-tuned-type controllers using PSO. The weighted modified PID has been applied to the voltage and current-tracking control of the same EV battery charger scheme for performance comparison. Matlab–Simulink software was used to design, test and validate the effectiveness of battery charger scheme using PV–FC renewable generation system with the GPFC device. The digital dynamic simulation model using Matlab–Simulink software environment allows for low-cost assessment and prototyping, system parameters selection and optimisation of control settings. The use of PSO-search algorithm is used in online gain adjusting to minimise controller absolute value of total error. This is required before full-scale prototyping, which is both expensive and time-consuming. The effectiveness of dynamic simulators brings on detailed sub-models selections and tested sub-models Matlab library of power system components already tested and validated. The common DC bus voltage reference is set at 1 PU. Digital simulations are obtained with sampling interval $T_s = 20$ μs. To compare the global performances of all cases, the normalised mean-square error (NMSE) deviations between output plant variables and desired values, and is defined as

$$\mathrm{NMSE}_{V_{\mathrm{DC-bus}}} = \frac{\sum (V_{\mathrm{DC-bus}} - V_{\mathrm{DC-bus-ref}})^2}{\sum (V_{\mathrm{DC-bus-ref}})^2} \quad (23)$$

$$\mathrm{NMSE}_{I_{\mathrm{DC-bus}}} = \frac{\sum (I_{\mathrm{DC-bus}} - I_{\mathrm{DC-bus-ref}})^2}{\sum (I_{\mathrm{DC-bus-ref}})^2} \quad (24)$$

The digital simulation results validated the effectiveness of PSO-based controllers in providing efficient energy utilisation, fast charging and stabilised DC chopper. The PSO-based self-tuned controllers are more effective and dynamically advantageous in comparison with the fixed gain-type controller. The control system comprises the three dynamic multi-loop error-driven regulators and is coordinated to minimise the selected objective functions. The weighted single-objective function combines several objective functions using specified or selected weighting

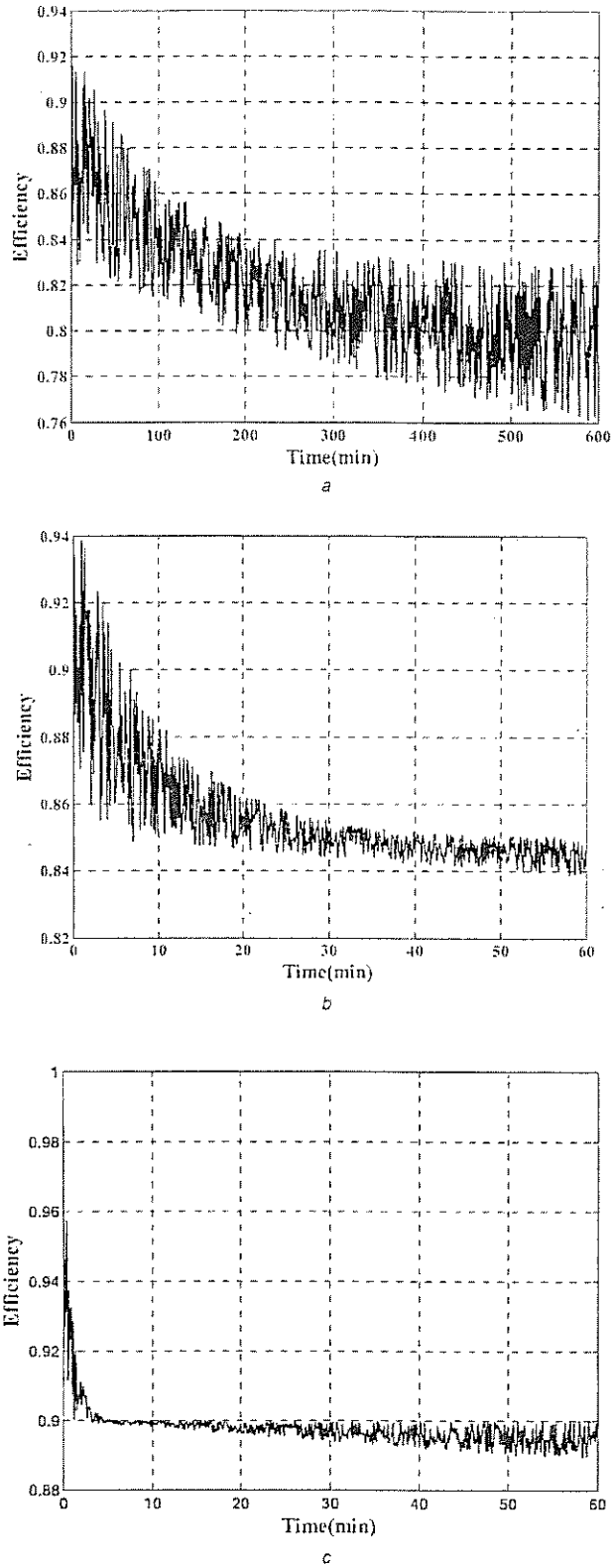

Fig. 6 *Battery-charger efficiency*
a Fixed gains weighted PID controller
b Self-tuned SOPSO-based controller
c Self-tuned MOPSO-based controller

doi: 10.1049/iet-est.2011.0021

factors as follows

$$\text{weighted objective function} = \alpha_1 J_1 + \alpha_2 J_2 + \alpha_3 J_3 + \alpha_4 J_4 + \alpha_5 J_5 \quad (25)$$

where $\alpha_1 = 0.20$, $\alpha_2 = 0.20$, $\alpha_3 = 0.20$, $\alpha_4 = 0.20$ and $\alpha_5 = 0.20$ are the selected weighting factors. J_1, J_2, J_3, J_4 and J_5 are the selected objective functions.

The main tests included the efficiency of the charger station, the current THD generated by the charger and the

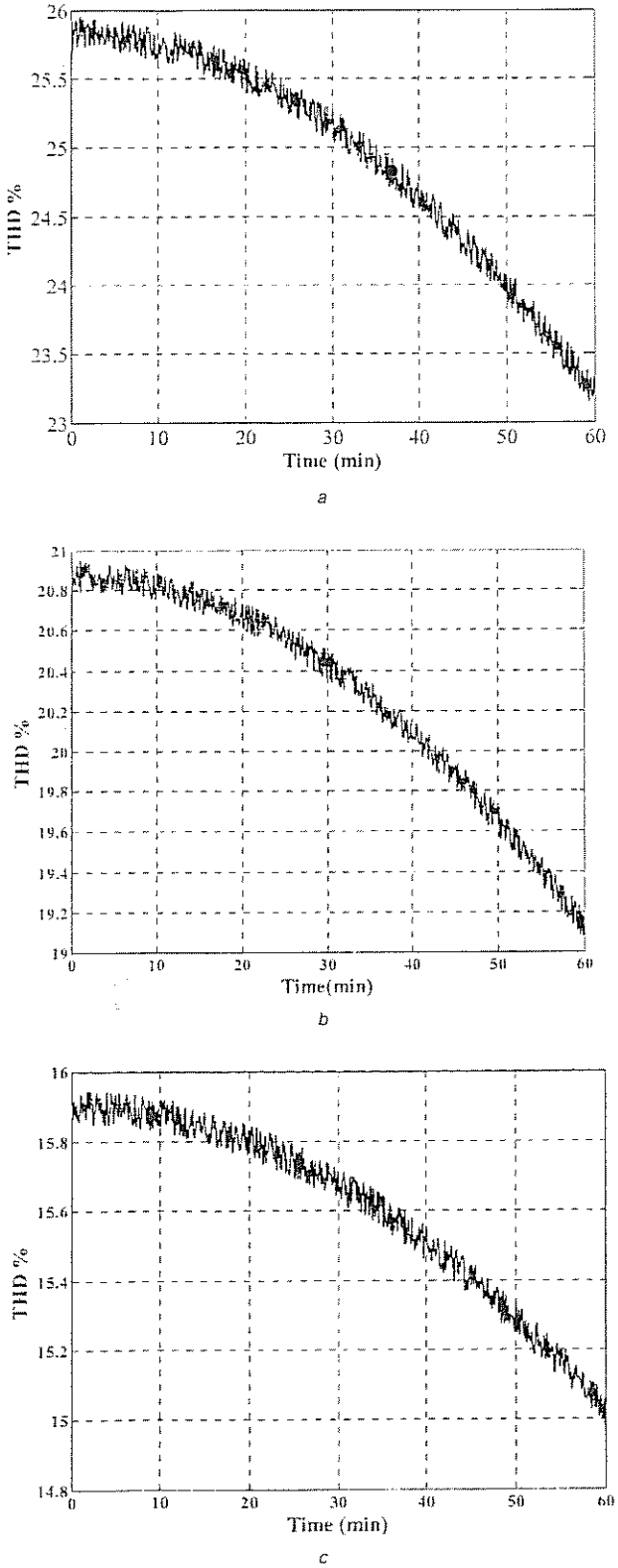

Fig. 7 *Measured input current harmonic distortion*

a Fixed gains weighted PID controller
b Self-tuned SOPSO-based controller
c Self-tuned MOPSO-based controller

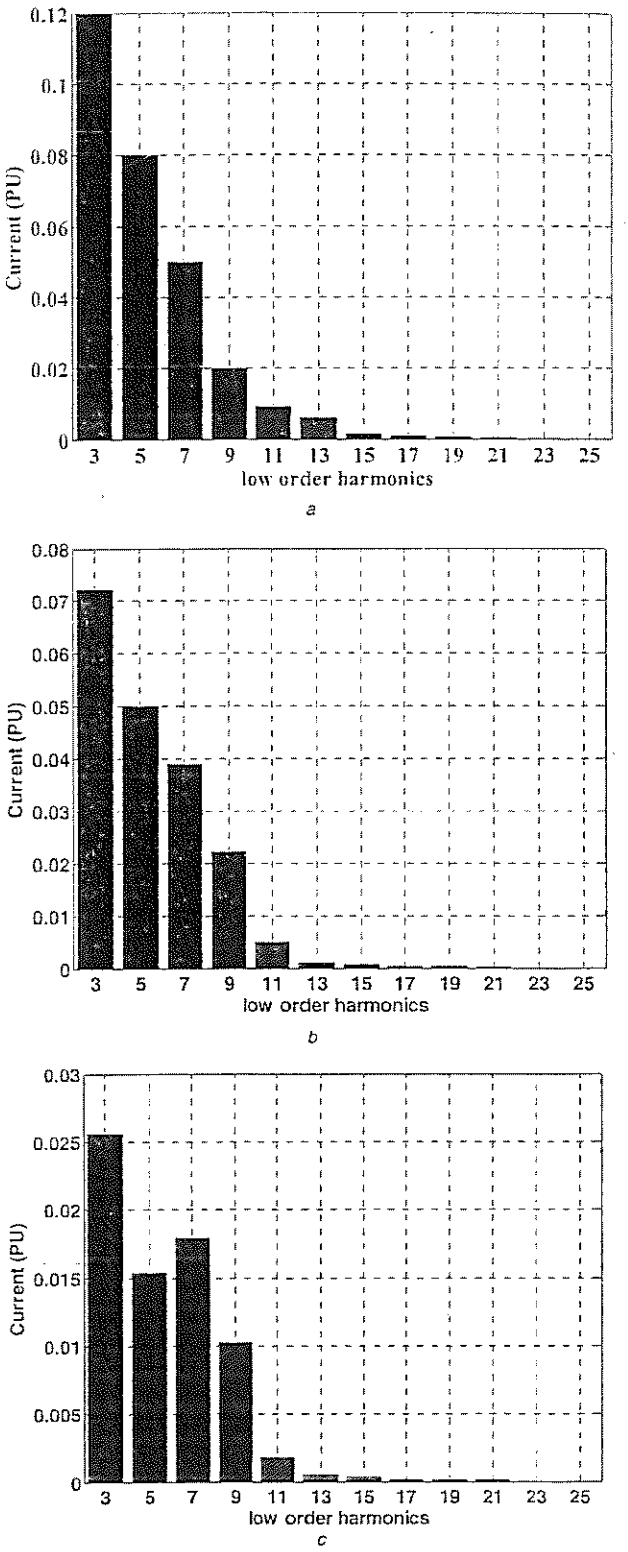

Fig. 8 *Output current low-order harmonics spectrum comparison*

a Fixed gains weighted PID controller
b Self-tuned SOPSO-based controller
c Self-tuned MOPSO-based controller

real power available from the source. Fig. 6 shows the measured charger efficiency during the charging period. The average charger efficiency during this test was 80% using fixed gains controller, 88.5% using single-objective particle swarm optimisation (SOPSO) and 92% using MOPSO. Figs. 7 and 8 illustrate the THD measurement on the charger input current (THD) during the same charging period. The charger produces less than 26% current THD at approximately 1 PU output using fixed gains controller, 20% current THD at approximately 1 PU output using SOPSO and 15% current THD at approximately 1 PU output using MOPSO. Comparing the behaviour of the proposed battery charging scheme using the fixed gains weighted modified PID controller, SOPSO and MOPSO-based self-tuned weighted modified PID controller, it is quite apparent that the PSO-tuning algorithms highly improved the battery-charging station performance from a general power quality point of view. Finally, Figs. 9 and 10 show the NMSE deviations comparisons of the battery voltage and current.

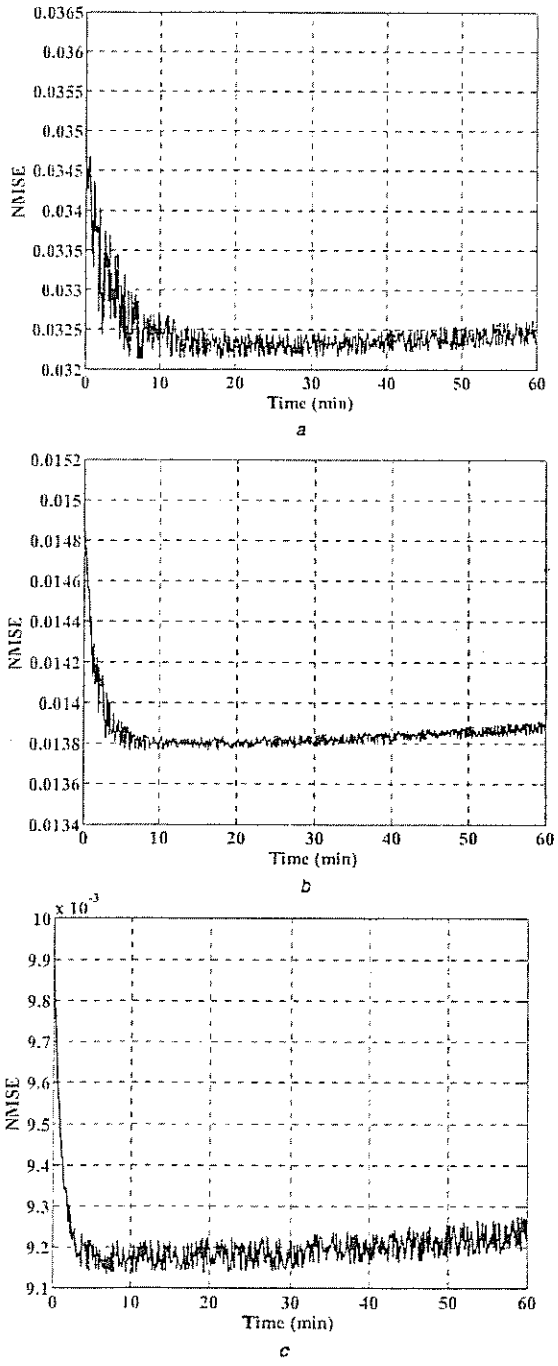

Fig. 9 *NMSE deviations comparison of the battery current*

a Fixed gains weighted PID controller
b Self-tuned SOPSO-based controller
c Self-tuned MOPSO-based controller

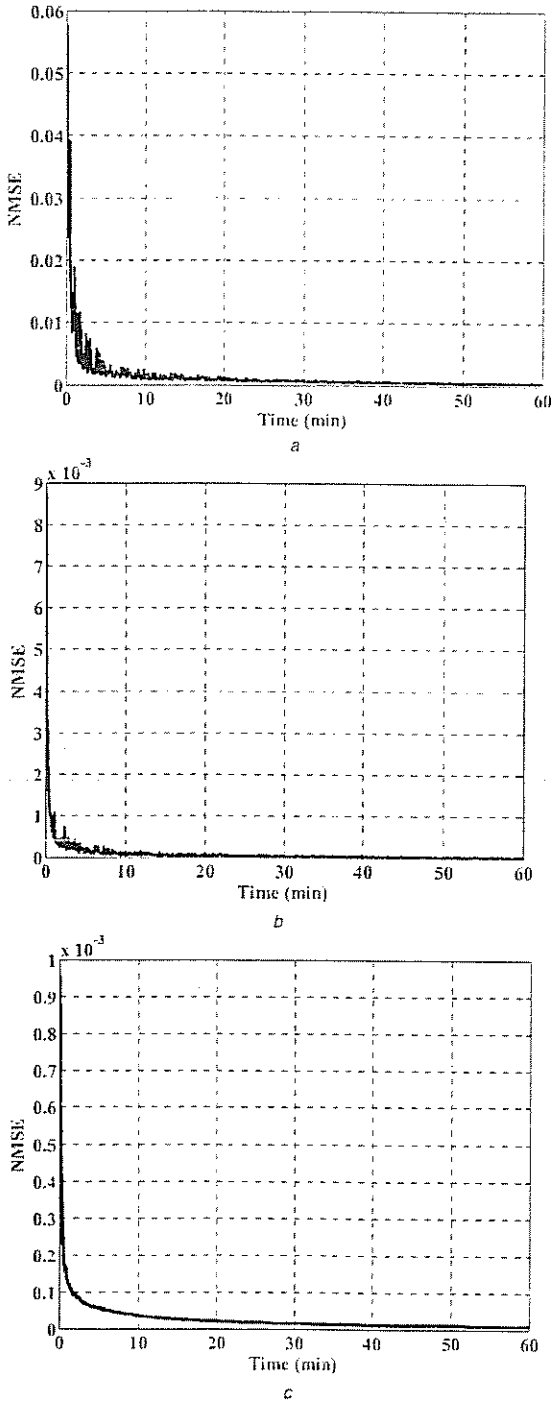

Fig. 10 *NMSE deviations comparison of the battery voltage*

a Fixed gains weighted PID controller
b Self-tuned SOPSO-based controller
c Self-tuned MOPSO-based controller

doi: 10.1049/iet-est.2011.0021

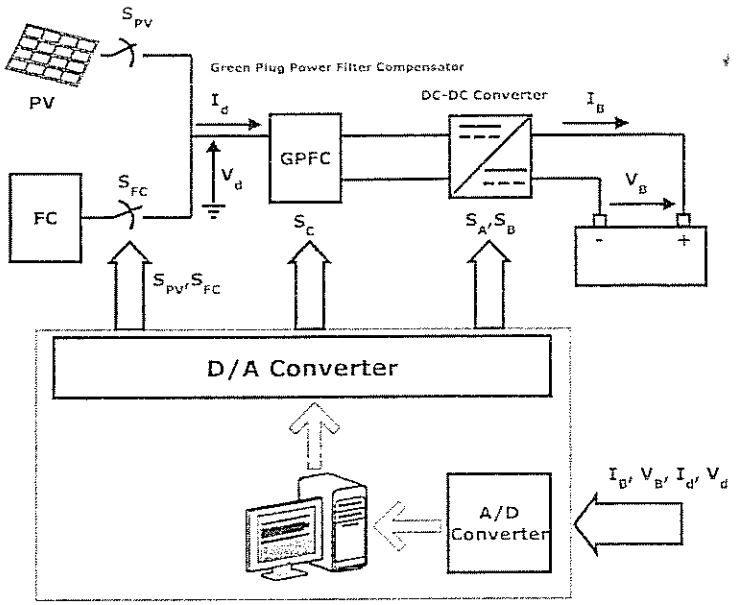

Fig. 11 *Experiment setup of the PV–FC battery charger*

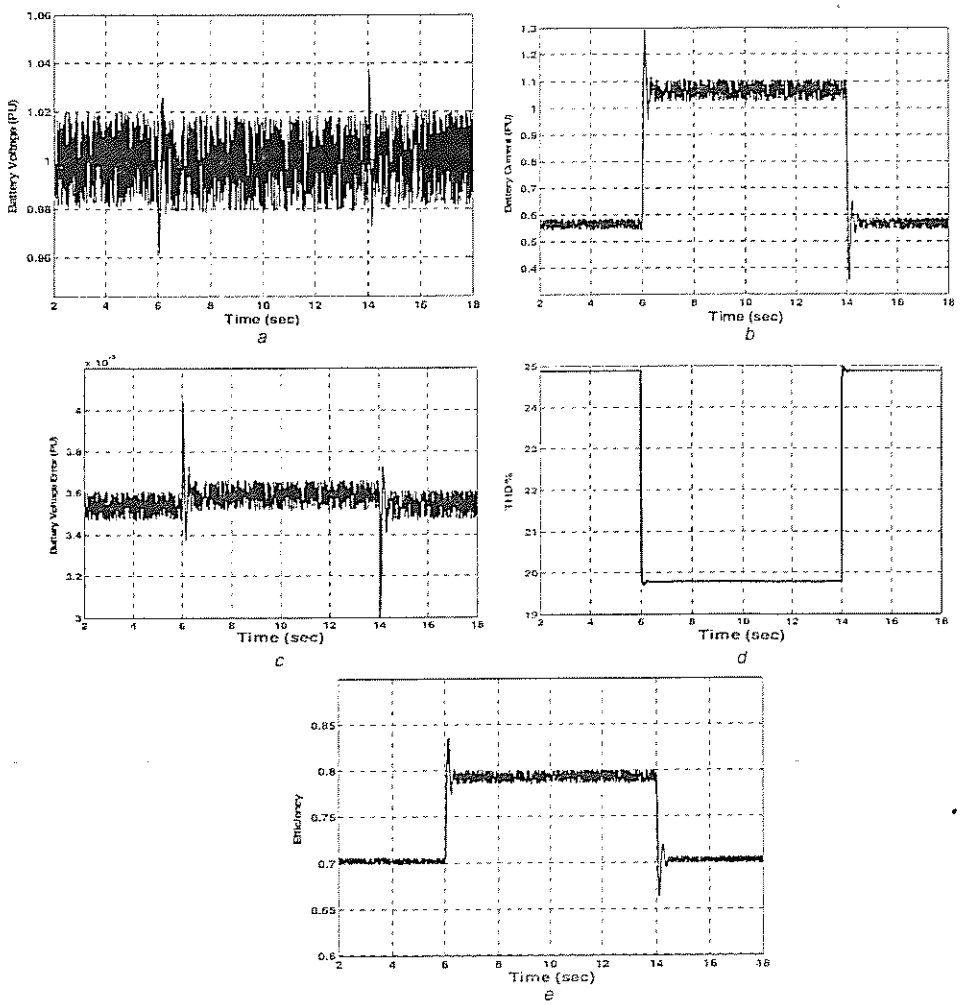

Fig. 12 *Experimental results with changing load for fixed gains weighted PID controller*

a Battery voltage
b Battery current
c Battery voltage error
d THD
e Efficiency

5 Experimental laboratory results

The laboratory prototype is shown in Fig. 11 to test the proposed controller performance. The main parts of the hardware setup are: microcomputer equipped with interface cards to execute the proposed controller algorithm, interface cards for A/D and D/A converter, two current transducers to measure the battery and DC bus currents, two voltage transducers to measure the DC bus and battery voltages, limiting circuit of the input signal to PC and delay circuit (lockout circuit) and isolation circuit. The computer processor executes the proposed optimisation PSO

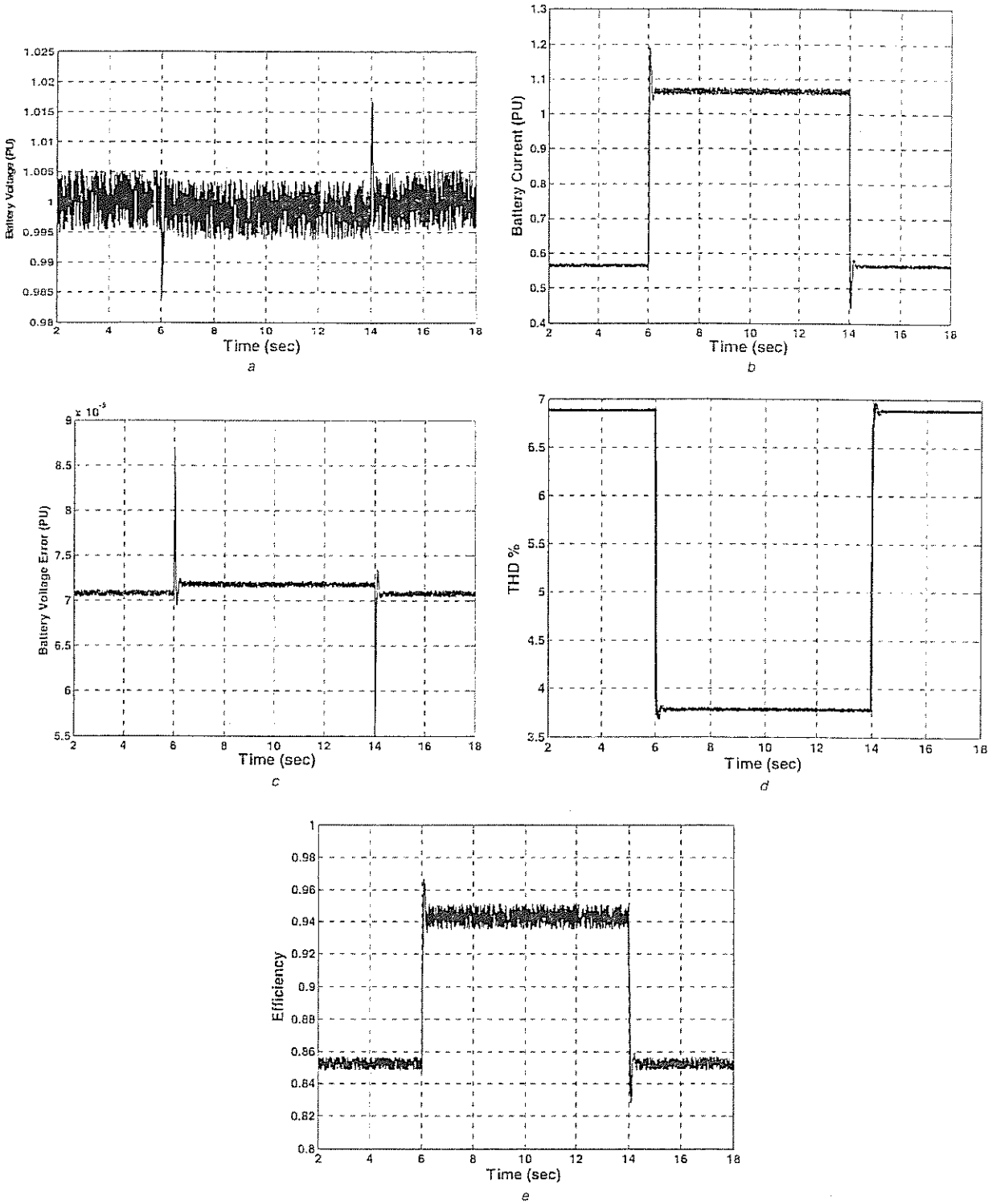

Fig. 13 *Experimental results with changing load for self-tuned MOPSO-based weighted PID controller*

a Battery voltage
b Battery current
c Battery voltage error
d THD
e Efficiency

doi: 10.1049/iet-est.2011.0021

controller, which is written in C language. The main tasks of the microcomputer is to Host the proposed PSO controller, which generates the switching state of the DC boost chopper, GPFC and energy management switching of PV and FC. The proposed battery charger consists of pulse width modulated (PWM) DC–DC boost converter and based on IGBTs for high performance and GPFC active filters for proper attenuation of current harmonics. The DC bus voltage V_{dc}, is chosen to 1 PU. A 2 kHz triangular carrier wave modulates the converters, which lead to a switching frequency, f_{sw} of 5 kHz. The controllers are sampled with a time interval, T, of 1 μs.

Figs. 12 and 13 show the battery voltage, battery current, battery voltage error, THD and system efficiency comparison for fixed gains weighted PID controller and self-tuned MOPSO-based weighted PID controller with load change from 0.5 to 1 PU. It can be seen that the THD is greatly reduced with the MOPSO control. The results show that at low loads the dc bus current can still achieve low harmonics; the THD of that DC bus current is around 3%. It can be noted that mains current THD are smaller than 6% from 50% load to full load. Finally, the proposed charger topology shows a high efficiency over entire load range and excellent input current harmonics.

Fig. 14 shows the changes of the PID controller gains and MOPSO execution time to attain a useful regulator gains as the load change from 0.5 to 1 PU. The search and optimisation time are very fast and it depends on the selection of stopping criteria (tolerance) and number of particles. The gain adjusting mechanism need not be

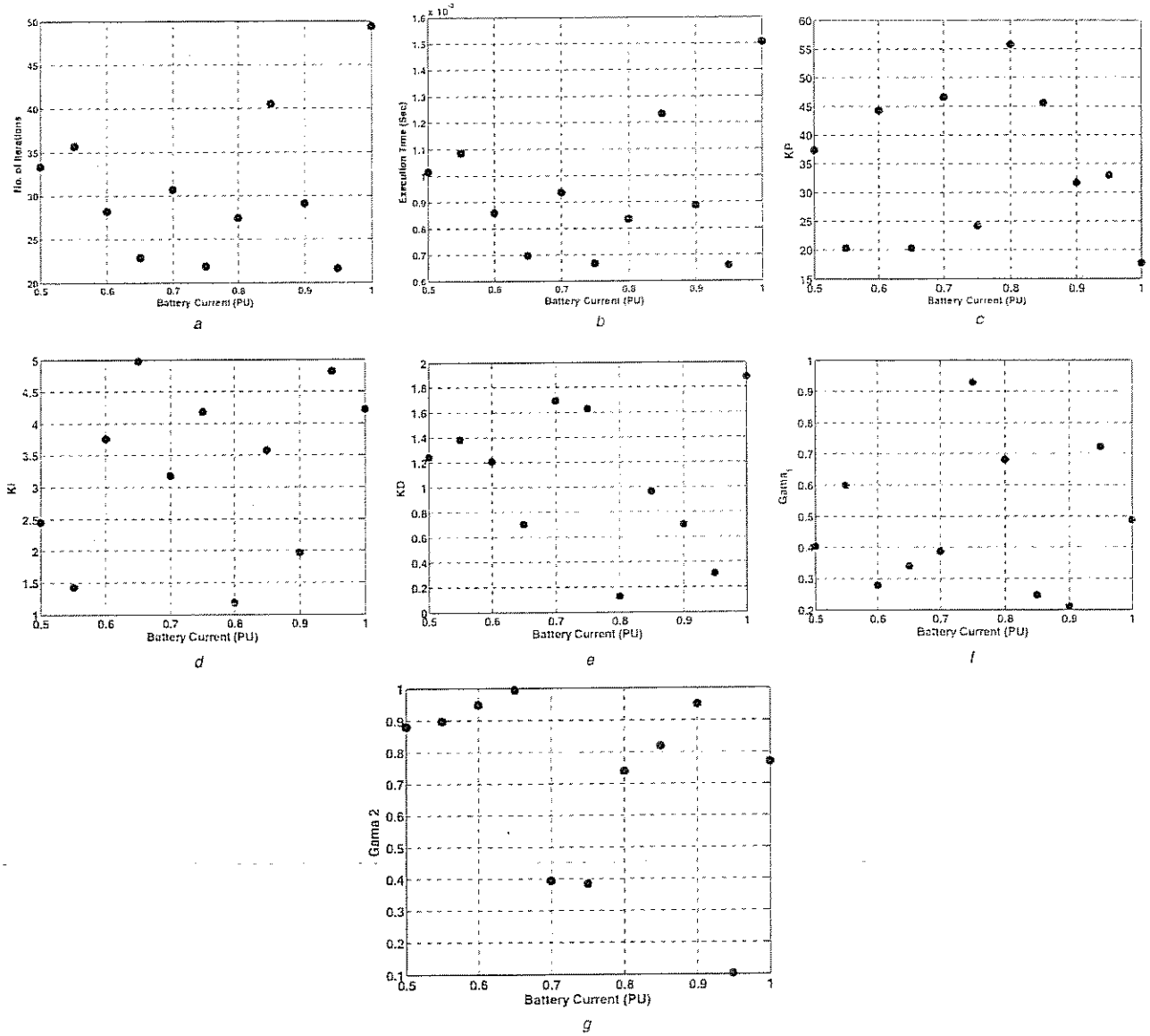

Fig. 14 *Optimal gains attained by the self-tuned MOPSO-based weighted PID controller:*

a Number of iterations
b Execution time
c K_P
d K_I
e K_D
f γ_1
g γ_2

applied at every sampling period but at fixed intervals to allow successful and complete search. The search and optimisation time in this case was ranging from 0.7 to 1.6 ms.

6 Conclusion

The paper validated a renewable green energy (PV–FC) utilisation dynamic scheme for vehicle-to-grid (V2G) battery-charging station. The charger scheme is coordinated by a tri-regulation controller with multi-loop error-driven modified and weighted PID controller. The coordinated multi-regulator control scheme is validated for hybrid PV–FC DC source load excursions and sudden DC source changes. Battery charging modes can be adjusted via weights and gains selections using the SOPSO and MOPSO hybrid charging modes. The goal of the MOPSO optimised tri-regulation scheme is to minimise the charging time, reduce current and voltage THD, enhance energy utilisation from the hybrid FC–PV renewable energy sources and maximise the real power available from the hybrid FC–PV renewable energy sources during the charging period. The proposed MOPSO tri-regulators can also ensure that the battery charger always utilise available DC source energy with minimal DC collection bus excursions. The self-adjusting coordinated tri-loop regulator with error-driven multi-loop structure and weighted loop contribution can ensure the stabilisation of the DC source collection bus and efficient energy operation.

7 References

1 Hajmiragha, A., Caizares, C.A., Fowler, M.W., Elkamel, A.: 'Optimal transition to plug-in hybrid electric vehicles in ontario, canada, considering the electricity-grid limitations', *IEEE Trans. Ind. Electron.*, 2010, **57**, (2), pp. 690–701

2 Maharjan, L., Inoue, S., Akagi, H., Asakura, J.: 'State-of-charge (SOC)-balancing control of a battery energy storage system based on a cascade PWM converter', *IEEE Trans. Power Electron.*, 2009, **24**, (6), pp. 1628–1636

3 Pellegrino, G., Armando, E., Guglielmi, P.: 'An integral battery charger with power factor correction for electric scooter', *IEEE Trans. Power Electron.*, 2001, **25**, (3), pp. 751–759

4 Wang, C.-W., Stielau, O.H., Covic, G.A.: 'Design considerations for a contactless electric vehicle battery charger', *IEEE Trans. Ind. Electron.*, 2005, **52**, (5), pp. 1308–1314

5 Egan, M.G., O'Sullivan, D.L., Hayes, J.G., Willers, M.J., Henze, C.P.: 'Power- factor-corrected single-stage inductive charger for electric vehicle batteries', *IEEE Trans. Ind. Electron.*, 2007, **54**, (2), pp. 1217–1226

6 Zhou, X., Wang, G., Lukic, S., Bhattacharya, S., Huang, A.: 'Multi-function bi-directional battery charger for plug-in hybrid electric vehicle application'. IEEE Energy Conversion Congress and Exposition, ECCE, 2009, pp. 3930–3936

7 Zhou, X., Lukic, S., Bhattacharya, S., Huang, A.: 'Design and control of grid-connected converter in bi-directional battery charger for plug-in hybrid electric vehicle application'. IEEE Vehicle Power and Propulsion Conf., 2009. VPPC'09, pp. 1716–1721

8 Musavi, F., Eberle, W., Dunford, W.G.: 'A high-performance single-phase AC-DC power factor corrected boost converter for plug in hybrid electric vehicle battery chargers'. IEEE Energy Conversion Congress and Exposition (ECCE), 2010, pp. 3588–3595

9 Sul, S.-K., Lee, S.-J.: 'An integral battery charger for four-wheel drive electric vehicle', *IEEE Trans. Ind. Appl.*, 1995, **31**, (5), pp. 1096–1099

10 Solero, L.: 'Nonconventional on-board charger for electric vehicle propulsion batteries', *IEEE Trans. Veh. Technol.*, 2001, **50**, (1), pp. 144–149

11 Jackson, D.K., Schultz, A.M., Leeb, S.B., Mitwalli, A.H., Verghese, G.C., Shaw, S.R.: 'A multirate digital controller for a 1.5-kW electric vehicle battery charger', *IEEE Trans. Power Electron.*, 1997, **12**, (6), pp. 1000–1006

12 Fakham, H., Lu, D., Francois, B.: 'Power control design of a battery charger in a hybrid active PV generator for load-following applications', *IEEE Trans. Ind. Electron.*, 2011, **58**, (1), pp. 85–94

13 Yamazaki, T., Muramoto, K.-I.: 'An advanced solar charging and battery discharge controller unit', *Renew. Energy*, 1998, **15**, (1), pp. 606–609

14 Dunlop, J.P.: 'Batteries and charge control in stand-alone photovoltaic systems, fundamentals and application' (Florida Solar Energy Center, Cocoa, FL, 1997)

15 Harrington, S., Dunlop, J.: 'Battery charge controller characteristics in photovoltaic systems', *IEEE Aerosp. Electron. Syst. Mag.*, 1992, **7**, (8), pp. 15–21

16 Woodworth, J., Thomas, M., Stevens, J., *et al.*: 'Evaluation of the batteries and charge controllers in small stand-alone photovoltaic systems'. Proc. 24th IEEE Photovoltaic Specialist Conf., Waikoloa, HI, 1994, pp. 933–945

17 Fernandez, M., Ruddell, A.J., Vast, N., Esteban, J., Estela, F.: 'Development of a VRLA battery with improved separators and a charge controller for low cost photovoltaic and wind powered installations', *J. Power Sources*, 2001, **95**, (1/2), pp. 135–140

18 Masheleni, H., Carelse, X.F.: 'Microcontroller-based charge controller for stand-alone photovoltaic systems', *Sol. Energy*, 1998, **61**, (4), pp. 225–230

19 Barbarisi, O., Vasca, F., Glielmo, L.: 'State of charge Kalman filter estimator for automotive batteries', *Control Eng. Pract.*, 2006, **14**, (3), pp. 267–275

20 Wang, J., Cao, B., Chen, Q.: 'Combined state of charge estimator for electric vehicle battery pack', *Control Eng. Pract.*, 2007, **15**, (12), pp. 1569–1576

21 Kennedy, J., Eberhart, R.: 'Particle swarm optimization'. Proc. IEEE Int. Conf. on Neural Networks, 1995, vol. 4, pp. 1942–1948

22 Ngatchou, P., Zarei, A., El-Sharkawi, A.: 'Pareto multi objective optimization'. Proc. 13th Int. Conf. on Intelligent Systems Application to Power Systems, 6–10 November 2005, pp. 84–91

23 Berizzi, A., Innorta, M., Marannino, P.: 'Multiobjective optimization techniques applied to modern power systems'. 2001 IEEE Power Engineering Society Winter Meeting, January 28–February 1 2001

24 Coello Coello, C.A., Lechuga, M.S.: 'MOPSO: a proposal for multiple objective particle swarm optimization'. IEEE Proc. World Congress on Computational Intelligence, 2003, pp. 1051–1056

8 Appendix

Fuel cell: 250 KW, 280 V_{dc}, $R_{f2} = 0.05\ \Omega$, $L_{f2} = 5$ mH, $C_{FC} = 6000\ \mu$F, open-circuit voltage (V) = 280, nominal voltage = 220 V, nominal current = 157.27 A, nominal efficiency, 56%, nominal air flow = 1300 l/pm, operating temperature = 65°C, nominal fuel pressure 1.5 bar, nominal air pressure = 1 bar.

PV energy system model: 300 KW, 280 VDC, $R_{f1} = 0.05\ \Omega$, $L_{f1} = 5$ mH, $C_{PV} = 6000\ \mu$F.

DC boost chopper: $R_o = 0.075\ \Omega$, $L_o = 2$ mH and $C_o = 4000\ \mu$F.

Battery: $R_B = 0.025\ \Omega$, $L_B = 2$ mH, V_B (maximum charging voltage) = 290 V, I_B (maximum charging current) = 400 A and SOC = 50%.

PMDC: 125 HP, 230 V, 120.4 rad/s, armature circuit resistance (R_a) 0.0125 Ω, armature circuit inductance (L_a) 0.065 H, moment of inertia (J) 3.0 kg/m^2, coefficient of friction (B) 0.60 N.M.s/rad, torque constant (K_T) 1.91 V.s/rad and Back–Emf constant (K_b) 1.91 V.s/rad

RL: 25 KW (heating/lighting)

GPFC: $R_s = 0.1\ \Omega$, $L_s = 10$ mH, $C_f = 3000\ \mu$F, $R_d = 0.2\ \Omega$, $L_d = 10$ mH, $C_d = 8000\ \mu$F and $R_{fd} = 20\ \text{K}\Omega$

Control weightings scaling: $\gamma_{V\ B} = 1$, $\gamma_{V\ B\ \text{dynamic}} = 0.75$, $\gamma_{V\ B\ \text{ripple}} = 0.5$, $\gamma_{I\ B} = 1$, $\gamma_{I\ B\ \text{dynamic}} = 0.75$, $\gamma_{I\ B\ \text{ripple}} = 0.5$, $\gamma_{P\ B} = 1$, $\gamma_{P\ B\ \text{dynamic}} = 0.75$, $\gamma_{P\ B\ \text{ripple}} = 0.5$, $0.01 < K_{V\ B} < 1$, $0.01 < K_{I\ B} < 1$, $0.01 < K_{P\ B} < 1$,

doi: 10.1049/iet-est.2011.0021

$0.01 < K_{I\ D} < 1$, $0.01 < K_{FD} < 1$, $\gamma_P = 1$, $\gamma_I = 0.75$ and $\gamma_P = 0.5$,

$T_1 = 5$, $T_2 = 5$, $T_3 = 5$, $T_4 = 5$, $T_5 = 5$, $T_6 = 5$, $T_7 = 5$, $T_8 = 5$, $T_9 = 5$, $T_{10} = 5$, $T_{11} = 5$, $T_{12} = 5$, $T_{13} = 5$ and $T_{14} = 5$ ms,

Self-tuned weighted modified PID controller: $1 < K_P < 100$, $0.1 < K_I < 10$, $0.1 < K_D < 5$, $0.1 < \gamma_1 < 4$ and $0.1 < \gamma_2 < 2$.

In the tuned weighted modified PID controller proposed controller scheme, the additional integral of the squared system error is implemented in this modified PID controller

$$u(t) = \gamma_1 \left(K_p e(t) + K_i \int_0^t e(t)\,\mathrm{d}t + K_d \frac{\mathrm{d}e(t)}{\mathrm{d}t} \right) + \gamma_2 (e(t))^2 \tag{26}$$

The modified PID controller gains (K_P, K_I, K_D, γ_1 and γ_2) are tuned using the PSO-searching algorithm to minimise the selected objective functions (J_1–J_5).